Journal of Nuclear Materials 508 (2018) 237–248

Contents lists available at ScienceDirect

Journal of Nuclear Materials

journal homepage: www.elsevier.com/locate/jnucmat

Wetting of liquid lithium on fusion-relevant materials microtextured by femtosecond laser exposure

S. Hammouti [a], B. Holybee [a], M. Christenson [a], M. Szott [a], K. Kalathiparambil [a], S. Stemmley [a], B. Jurczyk [b], D.N. Ruzic [a, *]

[a] Center for Plasma-Material Interactions, University of Illinois at Urbana Champaign, 201 S Goodwin Avenue, Urbana, IL, 61801, USA
[b] Starfire Industries, LLC, 2109 S Oak St, Champaign, IL, 61820, USA

ARTICLE INFO

Article history:
Received 31 October 2017
Received in revised form
19 May 2018
Accepted 23 May 2018
Available online 24 May 2018

Keywords:
Femtosecond laser
Plasma facing components
Lithium
Ripples
Wettability

ABSTRACT

As the use of liquid metals in plasma facing components becomes more widespread, it is important to investigate how these liquid metals interact with the surfaces onto which they are deposited. An important example of these interactions is the ability to control liquid metal wettability on fusion relevant substrates. In this work, we explore the influence of femtosecond laser induced nanostructured surfaces on the wetting degree of liquid lithium versus temperature. Three material candidates as a lithium wall in magnetic fusion devices have been investigated: molybdenum, tungsten and 304 L stainless steel. Laser parameters were tuned to induce periodical self-organized nanostructures (ripples or LIPSS) formation on each material. Wettability of laser treated materials was changed from lithium-philic to lithium-phobic for temperatures beyond 320 °C - 360 °C compared to untreated material. The effect of both laser induced topography and chemistry are quantified to explain the observed liquid lithium contact angles on each material. Finally, it was shown that topography in the form of self-organized periodical nanostructures as well as the surface chemistry in the form of oxides enrichment, both induced by a single step laser process, strongly influence the wetting degree of liquid lithium and enhance lithium-phobicity at high temperatures.

1. Introduction

Liquid metals received an increased attention within the plasma fusion community as an alternative solution to a critical technical challenge that solid plasma facing components represent. During magnetic fusion confinement experiments, the intense heat and particle fluxes produced by the plasma in the reactor vessel and encountered by solid Plasma Facing Components (PFC) can go up to 15 MW m^{-2} [1,2]. In these conditions, solid PFC – such as carbon or tungsten – will at best merely erode and at worst undergo nano-structuring events that if broken off can cause large influxes of material into the core plasma, or melting, causing macroscopic damage to the PFC tile [3,4]. In order to mitigate many of these issues, the use of molten liquid metal could prove a long-term solution by avoiding concerns about melting under off-normal transient events. Macroscopic damage to the PFC is no longer an issue as the liquid will rearrange itself back to its equilibrium configuration after any transient occurrence. A liquid lithium PFC offers several additional benefits to both the confinements of the plasma and to the heat handling abilities of the PFC [5]. The most commonly used material in the literature for liquid metal PFC is lithium. Lithium is the lightest alkali metal and it is very chemically reactive with the relevant ion species in fusion plasma including hydrogen, deuterium, tritium, carbon, and oxygen. The use of lithium on the walls of a fusion device leads to low core impurity concentrations due to its ability to getter impurities. Lithium is a low Z material, meaning that any lithium injected into the core will not greatly change the Z_{eff} of the core plasma, and low Z impurities – particularly lithium – will transport from the core easily [1]. The benefits of decreased impurities and a lower Z_{eff} have led to higher energy confinement times and more stable plasmas. Lithium has drawn a lot of interest recently and significant improvements of the plasma performance have been reported – both on tokamaks and stellarators, and reversed field pinches [6–10]. Therefore, wetting properties of liquid lithium appears as a major challenge. Flowing liquid metal PFC [11–15] and Capillary Pore System (CPS) PFC [16–18] represent

* Corresponding author.
E-mail address: druzic@illinois.edu (D.N. Ruzic).

https://doi.org/10.1016/j.jnucmat.2018.05.051
0022-3115/

the two main categories of experimented liquid PFCs in confinement devices. CPS is a liquid delivery system which allows liquid lithium to be introduced onto the surface of the PFCs through a passive capillary wicking system. The surface of the PFCs are designed to promote wetting as well as the wicking of liquid lithium. For example, T. F. Lin et al. used a Nd: VO4 laser texturing process to create open channels with various aspect ratios on both 316 L stainless steel and titanium-zirconium-molybdenum (TZM) [18]. The authors showed that laser textured surfaces promoted a passive but vigorous wicking and were fully wetted by molten lithium. At the University of Illinois at Urbana Champaign (UIUC), Ruzic et al. have developed and tested a liquid metal divertor called LiMIT. LiMIT employs thermoelectric currents flowing within the lithium, interacting with the main toroidal field of a fusion device [11]. During plasma operation, once the temperature gradient is established between the top (lithium surface) and the bottom of the trenches which composed the divertor, a thermoelectric current drives the liquid inside the trench due to the JxB force from the interaction of the thermoelectric current with the toroidal field. The flow is self-driven by the instantaneous thermal gradient, resulting in a self-adaptive process against the heat flow received from the plasma [11,19–23]. Nevertheless, the design of the LiMIT device requires liquid lithium wetting properties to be controlled accordingly. Lithium is expected to fully wet the inside of trenches and create a uniform liquid film which will enhance its flowing. Fiflis et al. already reported wetting properties of lithium on several potential candidates for liquid metal PFC and its dependence on temperature [24]. Since the ability to decrease the wetting temperature of lithium on different materials is crucial for a successful implementation of a flowing lithium divertor, it was shown that both plasma cleaning and lithium pre-coating are very effective in reducing the wetting temperature. In contrast, the surface of any liquid metal PFC must remain stable when exposed to the plasma and must accommodate or recover rapidly from conditions that could disrupt plasma performance. Rayleigh-Taylor and Kelvin Helmoltz instabilities as well as ELMy discharge can promote the ejection of liquid lithium droplets into the plasma [1]. In order to prevent lithium depositing in the periphery of the trenches in the LiMIT device during episodes of instabilities, the affinity between the trench surface area and liquid lithium is reduced by decreasing the wetting, increasing the contact angle between lithium and the material substrate. The strategy recently adopted at CPMI to create lithium-phobic surface on a wide range of materials was to develop a femtosecond laser surface texturing process. It is well known nowadays that ultrashort laser irradiation give access to nano/micro scale topography modification with a limited heat affected zone and —for certain laser conditions – induces self-organized periodical nano/microstructures called ripples or laser induced periodical surface structures (LIPSS) [25,26]. The mechanisms of ripple formation are still under investigation, but the functional aspect of surface modified by laser was widely demonstrated for many applications – especially for the control of surface wettability [27–30]. In this study, three different potential material candidates for liquid lithium wall – 304 L stainless steel, molybdenum, and tungsten – have been processed by femtosecond laser in order to obtain nanostructured surfaces for which liquid lithium wetting properties and the temperature dependence are then investigated under vacuum.

2. Experimental setup

2.1. Laser surface texturing process

Laser surface texturing was performed on three different materials: 304 L stainless steel, molybdenum and, tungsten. None of these materials were polished before laser treatment. A Coherent Monaco femtosecond diode pumped laser system with linearly polarized light was used for the laser processing of the material surfaces. This laser operates at a central wavelength of 1040 nm (Full Width at Half Maximum), pulse length 350 fs, at a maximum power of 40 W when the repetition rate is set to 1 MHz. A dual axis galvanometer system (GVS012(/M), Thorlabs) and a F-Theta lens (FTH160-1064, Thorlabs) were used to focus and steer the beam over the surface. The maximum field size is 110 × 110 mm with a repeatability of 5 μm. A schematic representation of the setup developed to perform 2D laser surface texturing is shown Fig. 1. Software was developed under LabVIEW in order to control the pattern of the texturing based on an imported image. Dimension of the texturing in both X and Y axis is related to the number of pixels which compose the image while the number of pulses delivered per spot is proportional to the value of each pixel. For this purpose, both of the galvanometer's drivers that control the rotation of the mirrors are connected to a 9269 NI DAQ card and the gate of the laser system is connected to a 9401 NI digital module. The peak fluence was calculated from Equation (1), assuming a Gaussian beam shape [31]:

$$F = \frac{2P}{f\pi\left(\omega_0/2\right)^2}\ [J.cm-2] \quad (1)$$

Where P is the laser power, f the repetition rate, and ω_0 the radius of the beam spot at $^1/_{e^2}$. The repetition rate, f, remained unchanged for all laser treatments and set at 1 MHz ω_0 was assessed by the technique developed and described by Liu [32]. This technique consists of analyzing a series of laser impacts made by varying the energy of the beam and then determining the size of the beam from the corresponding size of the impacts obtained in the ablative regime. The spot size was found to be around 60 μm. Areas of 40 mm × 10 mm were processed by laser on 304 L stainless steel and tungsten, and 35 mm × 10 mm on molybdenum by keeping constant the lateral displacement of the laser spot at 50 μm in both X and Y axis. Laser texturing was repeated on 4 samples for each investigated material. The observations of surface morphologies after laser irradiation were performed by scanning electron microscopy (SEM, JEOL 7000) and atomic force microscopy (AFM, Asylum Cypher) in tapping mode. Gwyddion software was used to visualize and investigate 3D AFM scans [33].

2.2. Wetting test setup and process

High energy surfaces of liquid metals are easily contaminated so care must be taken to maintain clean surfaces while measuring surface tension. Due to the highly reactive nature of lithium with many atmospheric species, experiments were conducted in vacuum to reduce oxidation rate [34,35]. The Materials Characterization Test Stand (MCATS) chamber at CPMI was specially designed to investigate the wetting phenomena of liquid metals on various fusion relevant substrates [24,36]. A 150 × 60 mm long movable stage mounted on a 20 mm thick plate heater allows for the controlled deposition of liquid metal droplets along the investigated surface by means of a manual linear travelling-screw that passes through an Ultra-Torr feedthrough. Lithium droplets were injected via a lithium injector composed of a piston, reservoir, tube, and nozzle. Prior to experiment, solid lithium is placed inside the reservoir of the injector which is then attached on top of the chamber. After loading the lithium, the chamber is pumped to vacuum and the injector is heated past lithium's melting point around 182.5 °C. A manual injector was developed that holds vacuum and allows a fine control over droplet size using a ramrod that

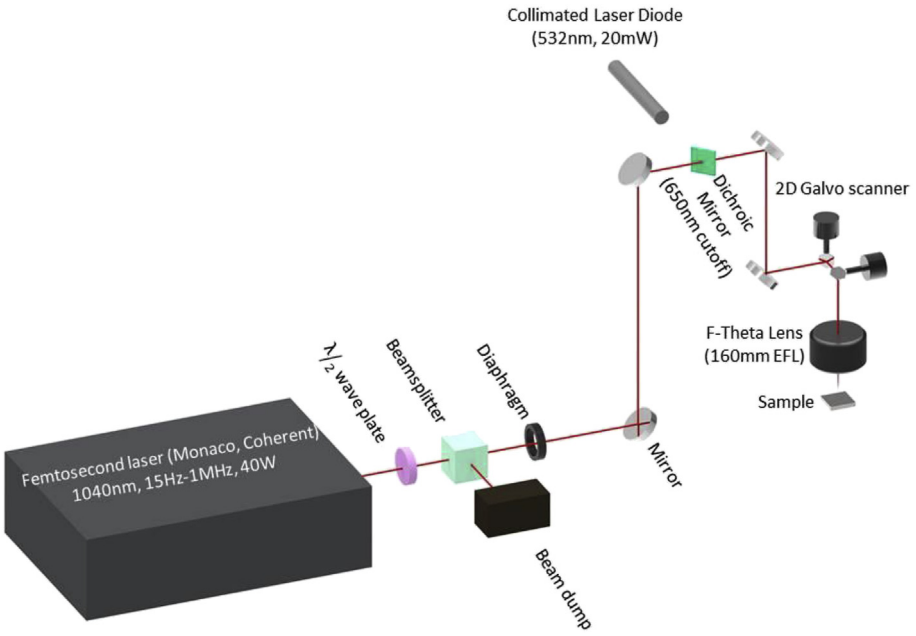

Fig. 1. Schematic representation of the setup used to perform 2D laser surface texturing.

passes out of the chamber through an Ultra-Torr vacuum feedthrough. The distance between the nozzle and the surface can also be adjusted manually during the experiment by means of a vertical rod attached below the plate heater which passes through an Ultra-Torr vacuum feedthrough. Since liquid lithium's wettability depends highly on the temperature of the substrate, temperatures of both injector and stage are setup by Variac variable transformers and controlled by means of thermocouples before droplet deposition and a new droplet is deposited for each temperature tested. Tests were performed at a mean pressure of 1.2×10^{-5} Torr. This pressure is rather satisfactory given both the manipulation of the lithium as well as the temperatures investigated. To overcome oxidation, at set intervals, the stage was moved and a new lithium droplet was placed to ensure that the surface of the lithium would be not be affected by oxidation during the photo capture time. Fig. 2 illustrates the lithium droplets deposition process in progress on femtosecond laser textured 304 L stainless steel surfaces. Silver paint was added at the sample-movable stage interface to enhance thermal conductivity. Experiments were performed between 250 °C and 450 °C in order to minimize surface evaporation of lithium.

Pictures of droplets were taken with a high-resolution camera (6000 × 4000 pixels) and a 500 W halogen bulb placed inside a ceramic tube behind the sample holder to ensure a good optical contrast. Pictures of droplets were then analyzed to determine the contact angle. This was done via the DropSnake plugin for Image J which is based on B-spline snakes (active contours) to shape the drop [37]. With this approach, the whole drop shape is used to provide global information; nevertheless, the contact angle measurement remains local and similar to a polynomial fit.

2.3. XPS measurements

To investigate the surface chemistry induced by femtosecond laser, XPS measurements were made using a Kratos Axis Ultra X-ray photoelectron spectrometer (Kratos Analytical, Inc., Manchester, UK) using monochromatic Al Kα radiation (1486.6 eV). High-resolution spectra were collected at a take-off angle of 90° using a pass energy of 40 eV from a 0.7 mm x 0.3 area using the hybrid (electrostatic and magnetic immersion) lens mode. The samples were affixed onto the sample holder using double-sided copper tape. The binding energy scale was referenced to the adventitious C 1s signal at 285.0 eV. The pressure during analysis was ca. 7 × 10-7 Pa. Collected XPS spectra were analyzed using CasaXPS software. After calibration, the background from each spectrum was subtracted using a Shirley-type background to remove most of the extrinsic loss structure. All survey scans were analyzed to determine the stoichiometry of the compound by using the appropriate

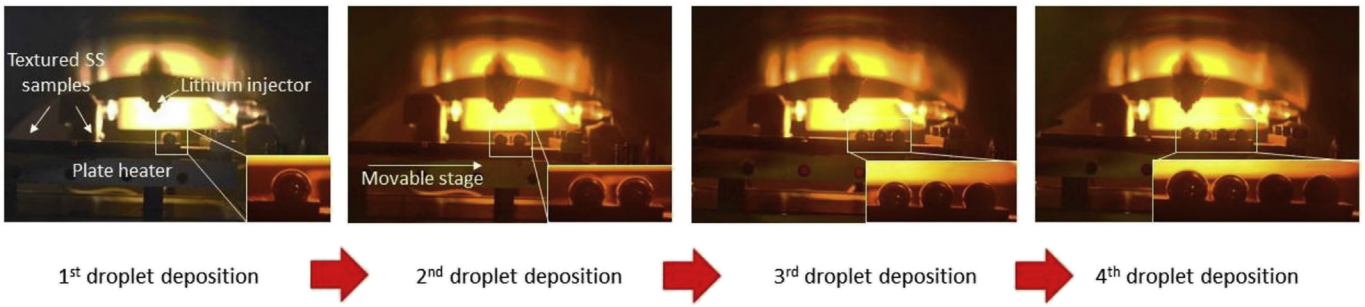

Fig. 2. Liquid lithium droplets deposition process used for wetting tests.

sensitivity factors and to determine the amount of adventitious carbon and contaminates present. High resolution XPS spectra was conducted based on data provided by literature for each material: 304 L stainless steel [38,39], molybdenum [40], and tungsten [41].

3. Results

3.1. Topographic characterization of surfaces processed by laser

Prior to performing any liquid lithium wetting test on laser textured samples, topographic analysis was conducted to characterize each material surface after laser treatment and ensure the presence of self-organized periodical nanostructures. The research of the relevant laser parameters to obtain LIPSS for each type of material was carried out experimentally. Test areas of 5 mm × 1 mm were first processed on each material for different laser power and number of pulses. Laser parameters were selected according to the morphologies observed on SEM images. Laser parameters used to perform surface texturing on each investigated material are in Table 1. For the liquid metal wetting tests, large surface areas (40mmx10 mm for 304 L stainless steel and tungsten, 35 mm × 10 mm for molybdenum) were processed by femtosecond laser and SEM images of nanostructures obtained on each material is showed Fig. 3.

Since it's important to investigate how liquid lithium interact with the surface onto which it is deposited, topographic parameters such as spatial periodicity of ripples and roughness parameters have been determined by AFM analysis. Fig. 3 shows AFM images of ripples on 304 L stainless steel, molybdenum, and tungsten – measured in tapping mode with a scan rate of 0.3 Hz. In all three sub-figures, the coverage of ripples appears quite uniform, although the ripple spatial periodicity is different for all laser treated surfaces.

According to the graph presented Fig. 4, 304 L stainless steel, molybdenum, and tungsten ripples have a periodicity of 800 ± 104 nm, 478 ± 86 nm, and 632 ± 65 nm, respectively. On can notice that the orientation of LIPSS is parallel to the direction of the laser polarization for all investigated materials. One of the critical parameters during the LIPSS formation is related to the laser polarization state. It is generally accepted that the irradiation with linear polarized laser radiation causes structures aligned perpendicular or parallel to the incident electric field (*E*-field) vector. LIPSS can be divided in two main categories. For normal incident radiation, Low Spatial Frequency LIPSS (LSFL) typically exhibits periods close to or slightly smaller than the irradiation wavelength ($\lambda/2 \leq \Lambda_{LSFL} \leq \lambda$), while High Spatial Frequency LIPSS (HSFL) have periods smaller than half of the irradiation wavelength ($\Lambda_{HSFL} < \lambda/2$) [25]. In this study, laser irradiation was performed at 1040 nm, therefore it seems that ripples measured on 304 L stainless steel and tungsten belong to the LSFL category while the ripples obtained on molybdenum belong to the HSFL category. Formation of LSFL can be explained either by the excitation of Surface Plasma Polariton (SPP) or related to the so-called Radiation Remnants (RR) [42,43], while the formation of HSFL can be related to mechanisms of self-organization or second harmonic generation (SHG) [44–46]. Due to the extreme complexity of the physical processes involved, especially after an ultrafast multi-pulse irradiation which includes feedback phenomena, LIPSS formation is still a current topic. The parameter R_{RMS} which is used as a global evaluation of the roughness amplitude on a profile doesn't vary a lot from one surface to another and was measured as 167 ± 45 nm, 135 ± 33 nm, and 111 ± 27 nm for 304 L stainless steel, molybdenum, and tungsten, respectively. Since the R_{RMS} parameter does not inform on the shape of the profile, assessing the skewness as well as the kurtosis is relevant as it provides complementary profile information [47]. The skewness corresponds to the asymmetry of the height distribution, defined on the sampling length. This parameter is important as it gives information on the morphology of the surface texture. Positive values correspond to high peaks spread on a regular surface (distribution skewed towards bottom) while negative values are found on surfaces with pores and grooves (distribution skewed towards top) which is the case for all investigated surfaces. Finally, the kurtosis parameter gives information on the sharpness of the height distribution, defined on the sampling length. Kurtosis values assessed for all surfaces are smaller than 3 which indicate broader height distributions unlike values greater than 3 which indicate a flattened surface topography.

Table 1
Laser parameters used for ripples generation on 304 L stainless steel, molybdenum and tungsten.

	Laser Power (W)	Fluence (J.cm^{-2})	Number of pulses
304 L Stainless steel	9	0.32	200
Molybdenum	7.5	0.27	12,000
Tungsten	8.5	0.30	15,000

3.2. Wetting tests on nanostructured surfaces

To conduct the wetting tests, 12 laser surface texturized samples were used: 4304 L stainless steel, 4 molybdenum, and 4 tungsten samples. Wetting experiments were achieved by testing one type of material at a time inside MCATS. Generally, 2 samples of the same material were loaded inside the vacuum chamber across the mobile stage and deposited on in succession. Multiple runs of wetting tests were needed to build up the results presented which provided overlap in the temperatures tested, verifying the results and displaying repeatability in the transition from non-wetting to wetting regimes. Contact angles of liquid lithium obtained on treated surfaces were compared to the ones previously reported by Filfils et al. for bare 304 L stainless steel, molybdenum, and tungsten [24] and recently confirmed by Szott [36].

The wettability of 304 L stainless steel, molybdenum, and tungsten surfaces was investigated through contact angle measurements. Figs. 5–7 depict the evolution of contact angles of liquid lithium as a function of temperature for 304 L stainless steel, molybdenum, and tungsten, respectively. Experiments were performed between 250 °C and 450 °C in order to minimize surface evaporation of lithium. From a global observation of the data obtained for all the treated materials, one can notice that all surfaces exhibit a lithium-phobic behavior (Θ>90°) for the entire range of temperatures tested and no wetting transition has been highlighted as it appears at 320 °C, 325 °C and 360 °C for untextured 304 L stainless steel, molybdenum, and tungsten surfaces respectively. Moreover, contact angles assessed on all type of textured surfaces are higher than the ones measured on untreated materials before the wetting regime. If one compare contact angles measured on fs laser treated surfaces, Fig. 6 shows that molybdenum surfaces exhibit the highest contact angles around 149.8° from 250 °C to 343 °C and shows a mean contact angle of 120.5 °C between 343 °C and 410 °C. In the case of textured tungsten surfaces (Fig. 7), evolution of contact angles is stationary between 250 °C and 361 °C with a mean around 140.7° and more varied between 361 °C and 411 °C with a mean contact angle of 118.5°. The last contact angle assessed for a stage temperature of 411 °C is close to the wetting transition and one can suppose that the wetting behavior of textured tungsten will transition from liquid lithium-phobic to liquid lithium-philic for higher temperatures. Finally, contact angles measured on fs laser treated 304 L stainless steel surfaces – shown Fig. 5 – are slightly lower than the ones characterized on

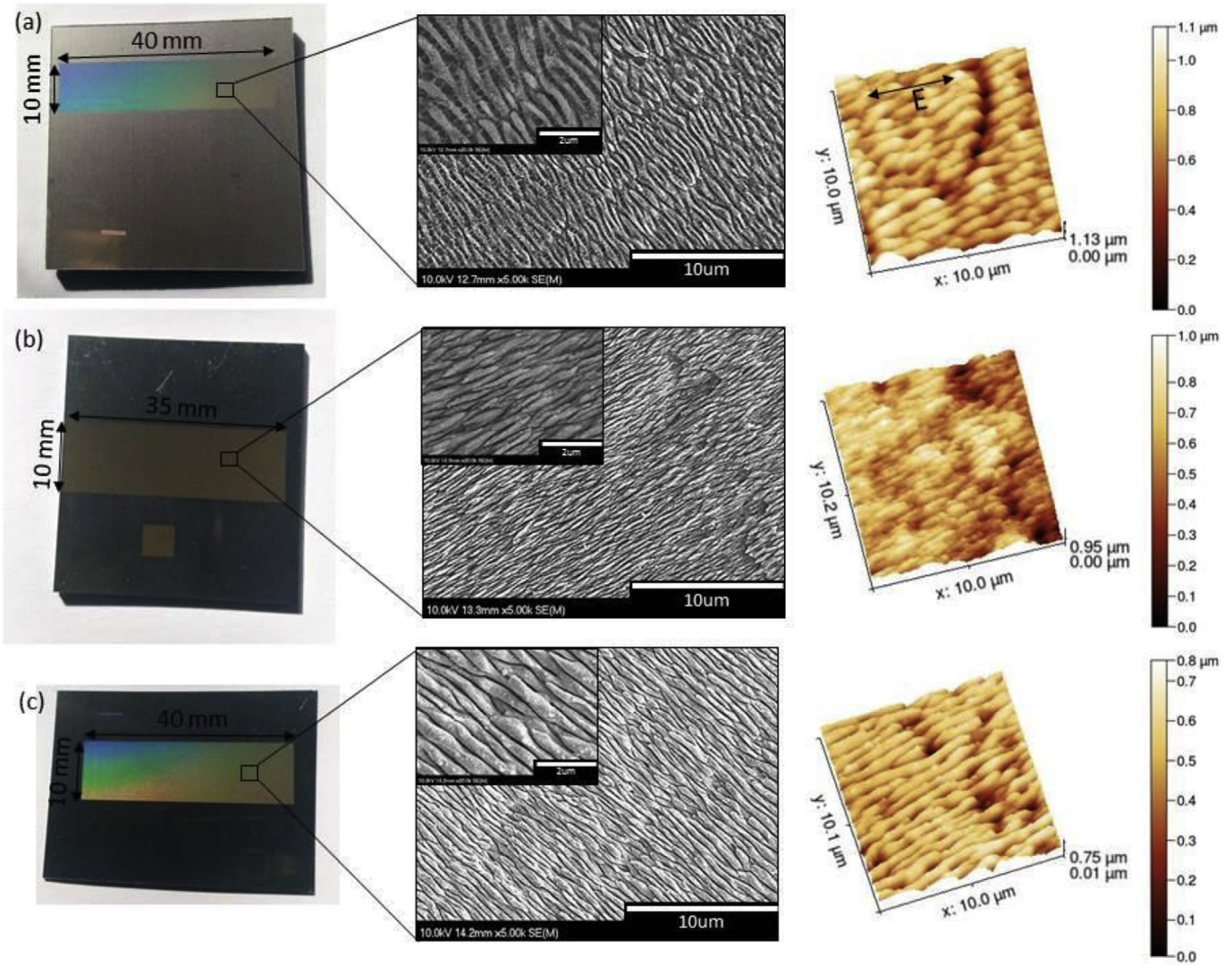

Fig. 3. (a) 5mmx1mm Laser surface texturing achieved on 304 L stainless steel for different number of pulses and laser power. Photos and SEM and AFM images of final laser surface texturing obtained on (a) 304 L stainless steel, (b) molybdenum and (c) tungsten.

previous texturing but appear to be constant with a mean around 116.5° in the temperature range tested.

4. Discussion

4.1. Influence of laser induced topography on lithium contact angles

From wetting measurements and topographic characterization of fs-textured surfaces, one correlation can be found between the mean contact angle (calculated for the range of temperatures tested) and the spatial periodicity of ripples. As shown Fig. 8, the ripple periodicity seems to have an influence on the mean contact angle and lower frequency surface structures appear to be favorable for higher liquid lithium-phobicity, which could be explained by one of the wettability models.

It's well known that the wetting properties between a liquid and a solid substrate can be modified by the roughness and phobic feature of a surface can be modulated by its texture as is the case in nature with the lotus leaf effect [48,49]. One way to assess the contribution of the topography generated by laser on the liquid lithium contact angles is to refer to wettability models. The intrinsic contact angle θ_Y in a non-reactive solid-liquid system is given by the classical equations of Young (Equation (2)) and Young-Dupré (Equation (3)) [50]:

$$\cos\theta_Y = \frac{\sigma_{SV} - \sigma_{SL}}{\sigma_{LV}} \tag{2}$$

$$\cos\theta_Y = \frac{W_a}{\sigma_{LV}} - 1 \tag{3}$$

Where the quantities σ_{SV} and σ_{LV} define the surface energy of the solid and liquid, respectively, and σ_{SL} defines the solid-liquid interface energy. W_a is the adhesion energy of the system defined as the energy required to separate reversibly a solid and a liquid having a common interface of unit area, creating two free surfaces, one solid-vapor and one liquid-vapor. Therefore, W_a is related to the surface energies of the system. Both Equations (2) and (3) give the "Young contact angle" θ_Y or intrinsic contact angle of a liquid on an ideal solid surface considered perfectly smooth and chemically homogeneous. Most of the time, chemical heterogeneities and the roughness of real solid surfaces lead to apparent contact angles which differ from θ_Y. Roughness of the solid surface

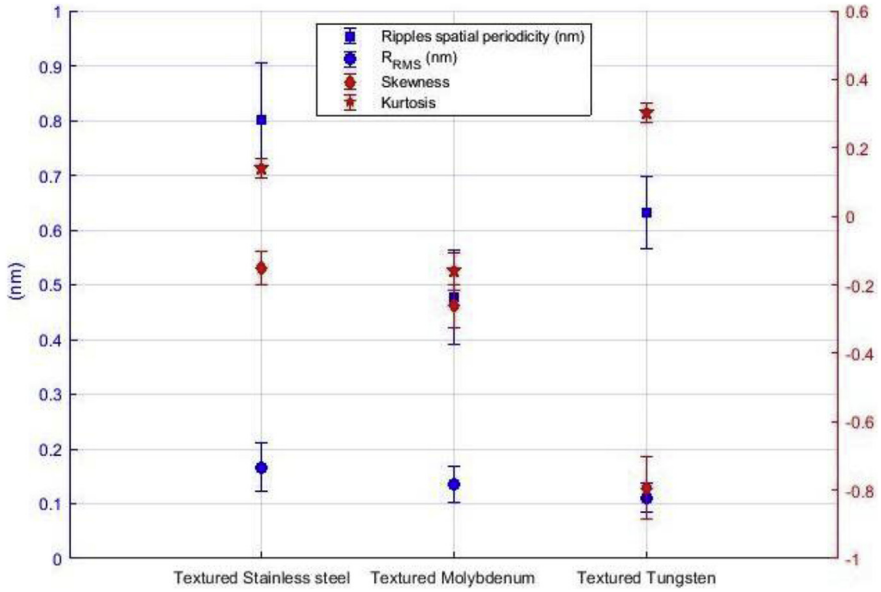

Fig. 4. Topographic parameters (ripples periodicity, R_{RMS}, Skewness and Kurtosis) assessed for each laser treated surface.

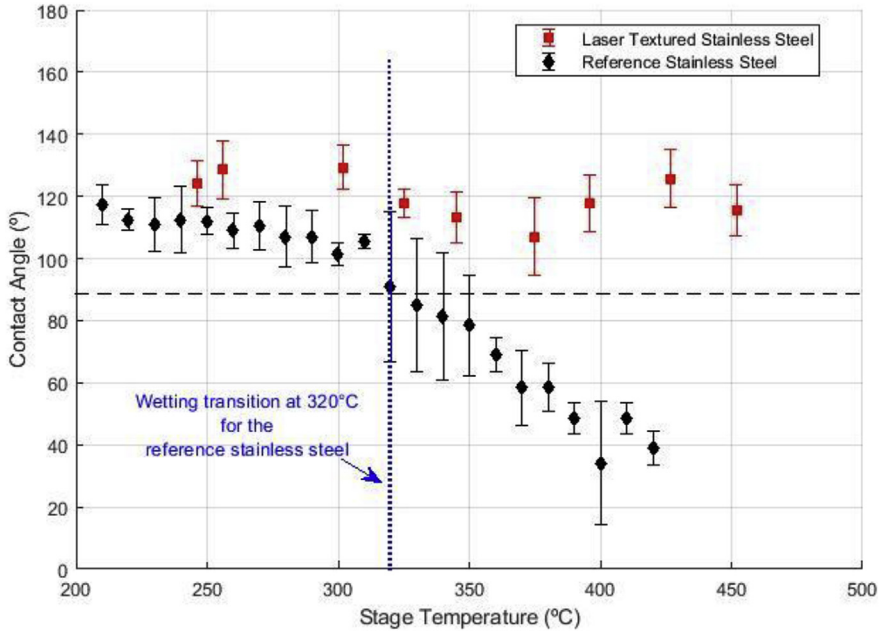

Fig. 5. Contact angles measurements of lithium on femtosecond laser treated304 L stainless steel. Wetting temperature occurs around 320 °C for untextured surface while laser textured sample still exhibits phobic behavior until 452 °C, maximum temperature reached during experiment.

affects wetting by increasing the actual surface area and pinning of the triple line by sharp defects. Contribution of roughness is expressed by Wenzel's equation [51]:

$$\cos\theta_W = r\cos\theta_Y \tag{4}$$

With r the ratio of the real area to the apparent area. Since r is equal or higher than 1, Equation (4) predicts that roughness will emphasize the phobic or philic character of a surface. Nevertheless, in the case of phobic surfaces ($\theta_Y >> 90°$), the formation of "composite interfaces", partly solid–liquid and partly solid–vapor, results in contact angles well above θ_Y. In this case, even limited stress produced during cooling leads to detachment of the solidified metal from the substrate by a purely adhesive rupture. When dealing with a heterogeneous surface roughness, the Wenzel model does not accurately describe the apparent contact angle. The Cassie-Baxter equation provides a better generalization of the Wenzel model. Cassie originally described the wetting case of a flat, chemically heterogeneous surface, and described the apparent contact angle as [52]:

$$\cos\theta_{CB} = r_1\cos\theta_1 + r_2\cos\theta_2 \tag{5}$$

where r_1 and r_2 are the area fractions which compose the total heterogeneous surface such as $r_1 + r_2 = 1$, with θ_1 and θ_2 the contact angles formed on each of these areas. Kramer et al.

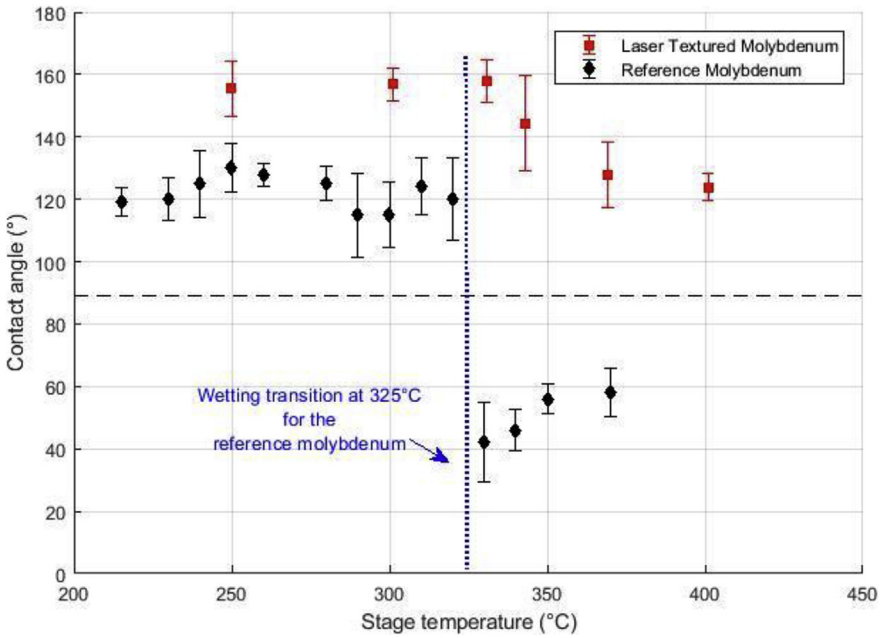

Fig. 6. Contact angles measurements of lithium on femtosecond laser treated molybdenum. Wetting temperature occurs around 325 °C for untextured surface while laser textured sample still exhibits a phobic behavior until 401 °C, maximum temperature reached during experiment.

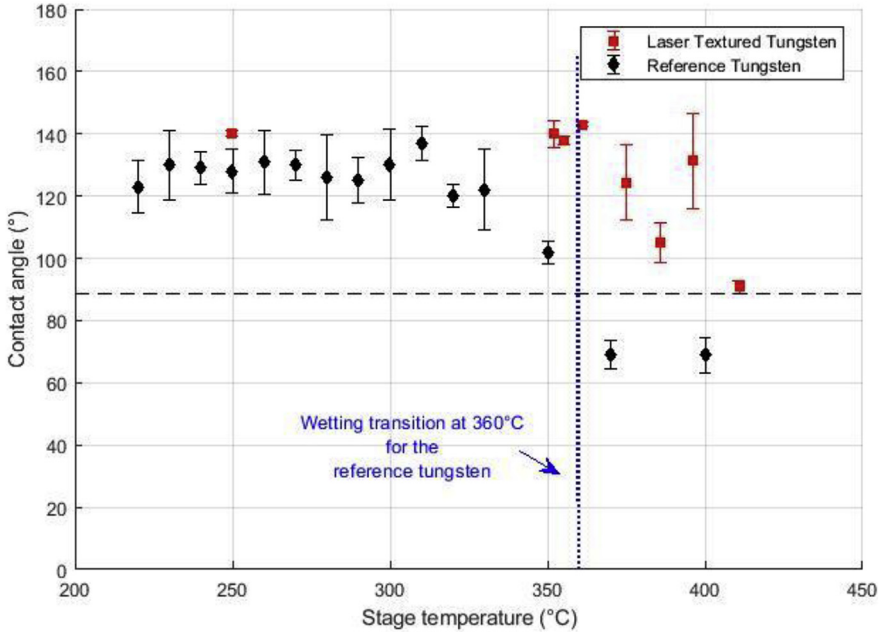

Fig. 7. Contact angles measurements of lithium on femtosecond laser treated tungsten. Wetting temperature occurs around 360 °C for untextured surface while laser textured surface still exhibits a phobic behavior until 411 °C, maximum temperature reached during experiment.

employed another version of Equation (5) to determine the applicability of the Cassie-Baxter relationship to the observed wetting behavior of eGaIn on microtextured indium surfaces [53]. If one applies this model to our study it leads to:

$$\cos\theta_{CB} = r\varphi\cos\theta_1 + (1-\varphi)\cos\theta_2 \quad (6)$$

Where $r\varphi$ and $(1-\varphi)$ are the areal ratios of the Li-textured surface and Li-air interface compared to the total droplet contact area, respectively. It was demonstrated that the parameter $(1-\varphi)$ can be approximated from the image processing of the surface topography. Thus, the AFM height images shown previously Fig. 3 were converted to binary images via the software Image J in order to isolate the pixels which correspond to the top of the laser induced surface structures ("foreground" pixels). The threshold level was adjusted manually until the structures with the highest height – which interact with the droplet surface – were present, shown in Fig. 9). Results are shown Table 2.

Assuming that the diffusion of lithium into the air gaps formed between ripples is negligible, the areal ratio of the Li-fs textured surface interface compared to the total droplet contact area can be

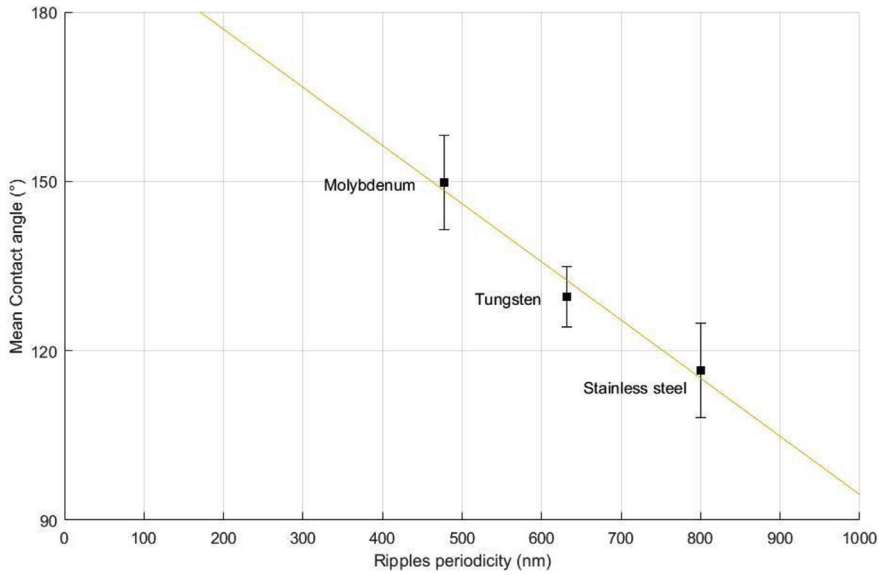

Fig. 8. Influence of the ripples periodicity induced after laser irradiation on the mean lithium contact angle. Simple linear fit was applied on data and a R-squared of 94.8% was obtained.

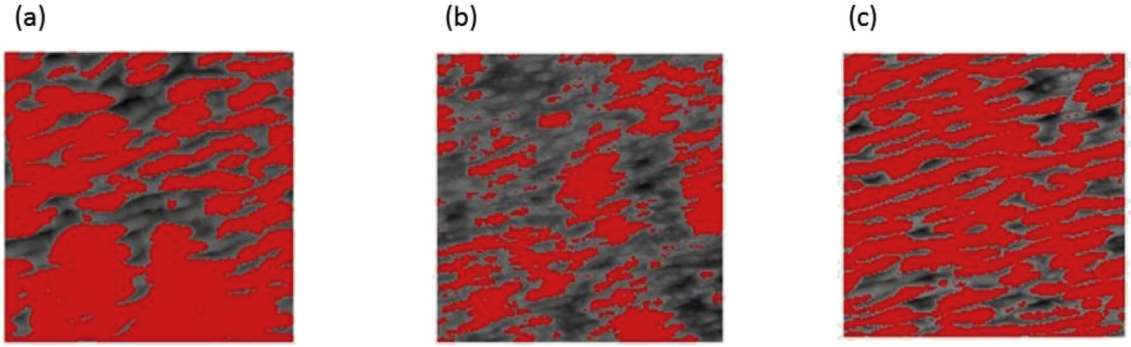

Fig. 9. Binary images obtained after AFM height images thresholding of (a) 304 L stainless steel, (b) molybdenum and (c) tungsten. Red area corresponds to the "foreground" pixels (peak of laser induced nanostructures), while the grey area corresponds to the "background" pixels. (For interpretation of the references to colour in this figure legend, the reader is referred to the Web version of this article.)

Table 2
Threshold values found for each laser surface texturing after image processing by binary conversion.

	Textured 304 L Stainless Steel	Textured Molybdenum	Textured Tungsten
Threshold level $(1-\varphi)$	$124/255 = 0.49$	$128/255 = 0.50$	$144/255 = 0.56$
$r\varphi \approx \varphi$	0.51	0.50	0.44

approximated by $r\varphi = \varphi$. If one substitutes the values found in Table 2 into Equation (6), the contact angles between lithium and untreated surfaces θ_1 can be estimated as shown in Table 3:

From the results presented in Table 3, the Cassie-Baxter relationship provides estimated contact angles differ from 5.3% up to 25% to the ones measured experimentally. It is clear from the observed contact angles of untextured and laser textured surfaces that introducing a nanometer scale pattern enhances lithiumphobicity. Cassie-Baxter model could explain the contact angles observed previously but surface chemistry induced by fs laser treatment has to be taken into account and assessed before and after laser irradiation.

Table 3
Comparison of the mean contact angles experimentally observed for each untreated material and the ones estimated from Equation (6).

	Experimental CA	Estimated CA
Untextured 304 L Stainless steel	86.3°±9°	91.1°
Untextured Molybdenum	102°±8°	125°
Untextured Tungsten	118°±7°	94.7°

4.2. Assessment of laser induced surface oxidation

All lithium deposition experiments were performed under high vacuum conditions which exclude the formation of an oxide layer around lithium droplet, however metallic solids are easily oxidized and their wettability by non-reactive metal is affected by oxide films that may be very tenacious even at high temperatures [54]. Since laser treatments were performed under atmospheric

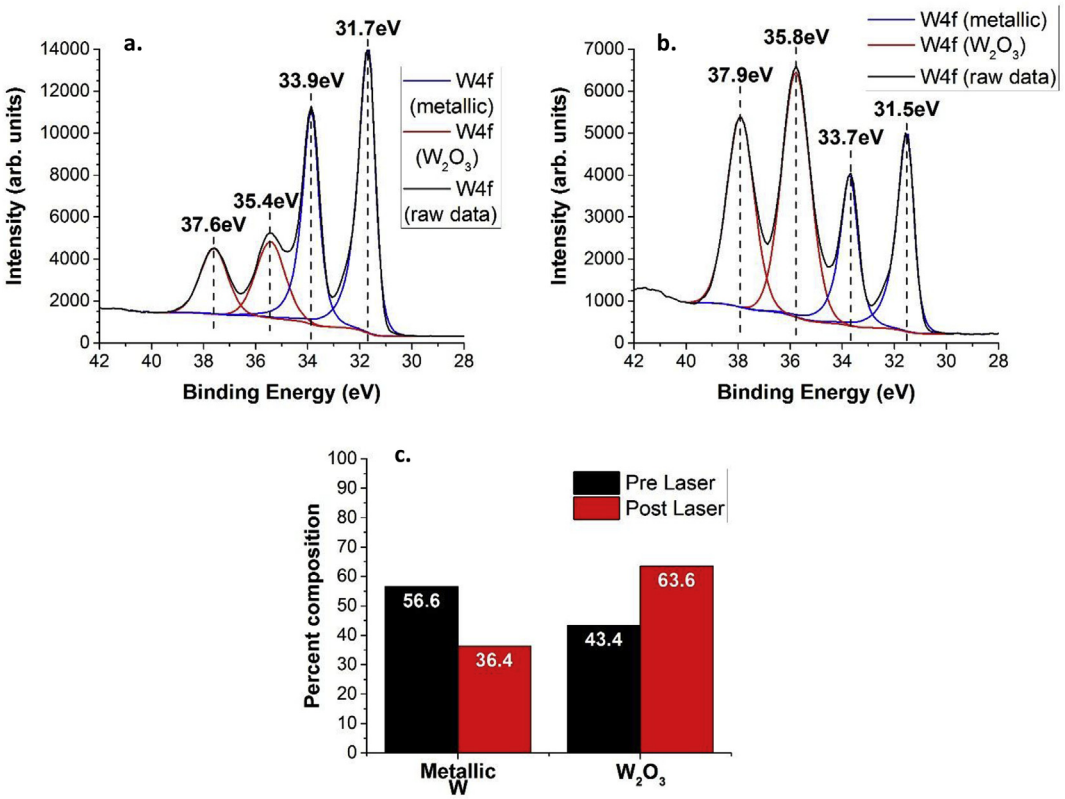

Fig. 10. XPS spectrum of W4f peaks for tungsten before laser irradiation (a) and after (b). Diagram of the surface composition in percentage of tungsten before and after laser irradiation (c) Inherent error from composition calculation is assessed around ±5%.

conditions at a high repetition rate, XPS analyses were conducted on all sample surfaces before and after laser processing to investigate laser oxidation. In order to oxidize a metal thin film, oxygen ions diffuse through the already-present passive oxide layer to react with the metal atoms to form the new oxide layer. The metal's atoms are excited due to the electronic regime from the femtosecond pulses [55]. Figs. 10–13 show XPS measurements for untreated and laser treated tungsten, 304 L stainless steel, and

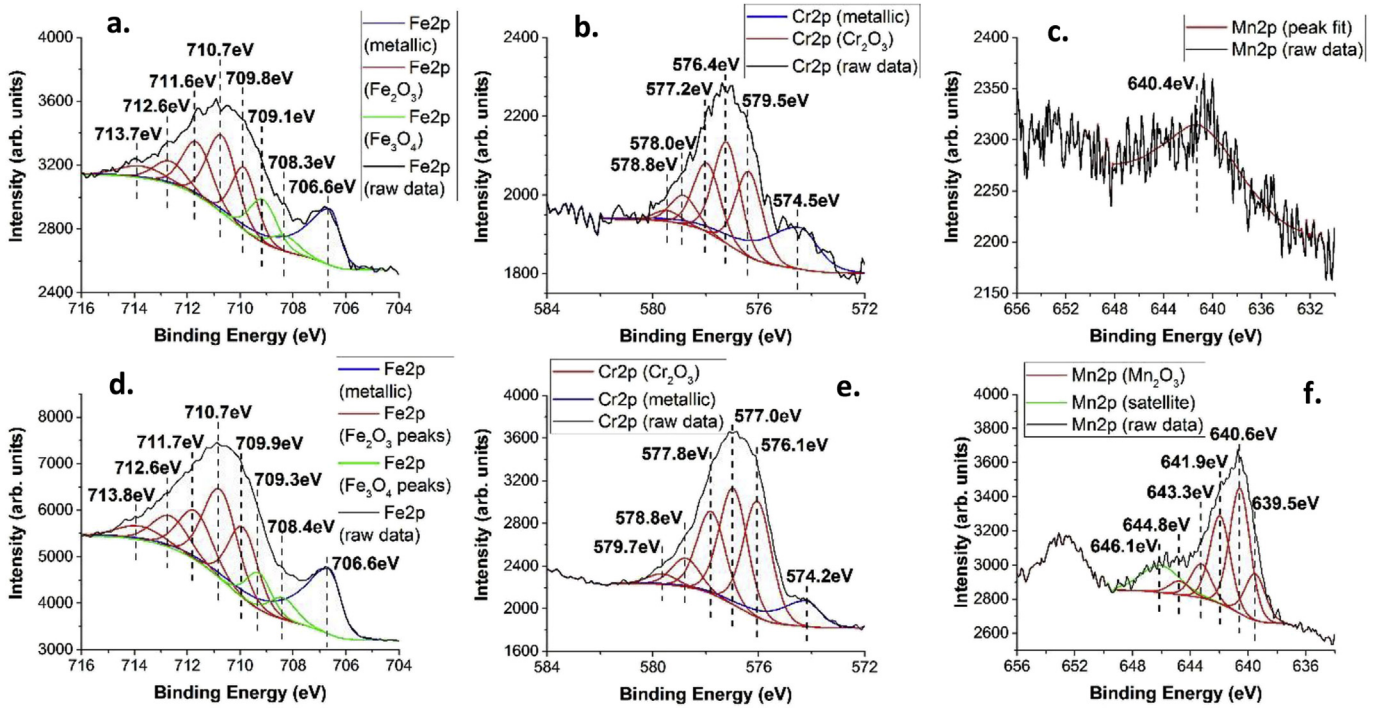

Fig. 11. XPS spectrum of Fe2p (a) Cr2p (b) and Mn2p (c) peaks for 304 L stainless steel before laser irradiation. XPS spectrum of Fe2p (d) Cr2p (e) and Mn2p (f) peaks for304 L stainless steel 304 after laser irradiation.

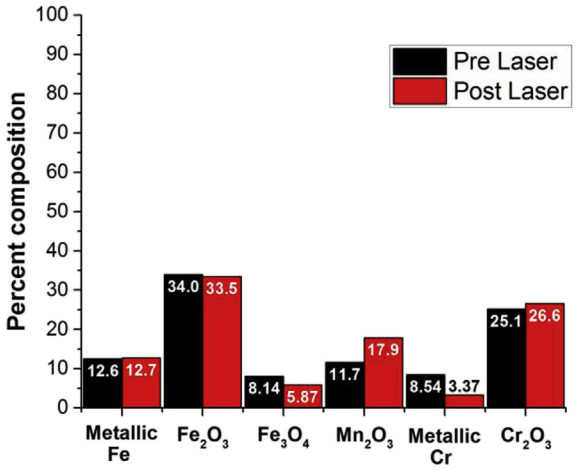

Fig. 12. Diagram of the surface composition in percentage of stainless steel 304 before and after laser irradiation. Inherent error from composition calculation is assessed around ±5%.

molybdenum surfaces, respectively. The XPS spectra of W4f peaks for tungsten samples before and after laser irradiation are shown Fig. 10(a) and (b) respectively. Before laser irradiation, the XPS spectrum of W4f is dominated by tungsten metallic peaks. After laser irradiation, the trend previously observed reverses with tungsten (IV) oxide (WO_3) peaks being stronger than the metallic peaks demonstrating the enrichment of oxides at the surface after laser irradiation. Fig. 10 (c) shows the composition in percentage of each compound which constitutes the analyzed surface depth and confirms the laser induced oxidation with a 20% increase of tungsten (IV) oxide (WO_3) in the final surface composition after laser irradiation.

XPS investigation of 304 L stainless steel surface is more complex since it involves the study of the chemistry of each element which composes the alloy. Fig. 11(a) and (b) and (c) show respectively the XPS spectra of Fe2p, Cr2p, and Mn2p peaks before laser irradiation, while Fig. 11(d) and (e) and (f) shows XPS spectra of the same peaks after laser irradiation. Fig. 11(a) and (b) show the existence of a passive film composed of Fe_2O_3, Fe_3O_4 and Cr_2O_3 on untreated surface. The corrosion resistance of stainless steel is known to be due to chromium oxide (Cr_2O_3) at the surface, which is considered to act as a protective layer against corrosion due to its low diffusion constants for oxygen and metal ions. The oxide layer formed on stainless steel surfaces is usually not uniform with depth. After laser patterning (Fig. 11(d) and (e) and (f)), the passive film still contains the same initial oxide components (Fe_2O_3, Fe_3O_4 and Cr_2O_3), but Mn_2O_3 is present in significant amounts as well. As shown Fig. 12, it seems that manganese has segregated from the bulk and has formed a significant contribution to the surface oxides after laser irradiation. Enrichment of chromium oxides at the surface also occurred. All these oxides participate in the inhomogeneous nature of the final passive film.

XPS measurements performed on molybdenum surfaces appear to be the most interesting in terms of oxide restructuring. Fig. 13(a) and (b) show XPS spectra of Mo3d peaks before and after femtosecond laser processing, respectively. Initially, the surface is dominantly composed of metallic molybdenum with a significant molybdenum (IV) trioxide (MoO_3) composition as shown in Fig. 13 (a). After laser irradiation, the metallic contribution is significantly reduced and multiple oxides formation is observed as shown Fig. 13 (b). XPS spectrum exhibits new peaks referred as molybdenum (II) oxide, molybdenum (IV) dioxide (MoO_2), and molybdenum (VI)

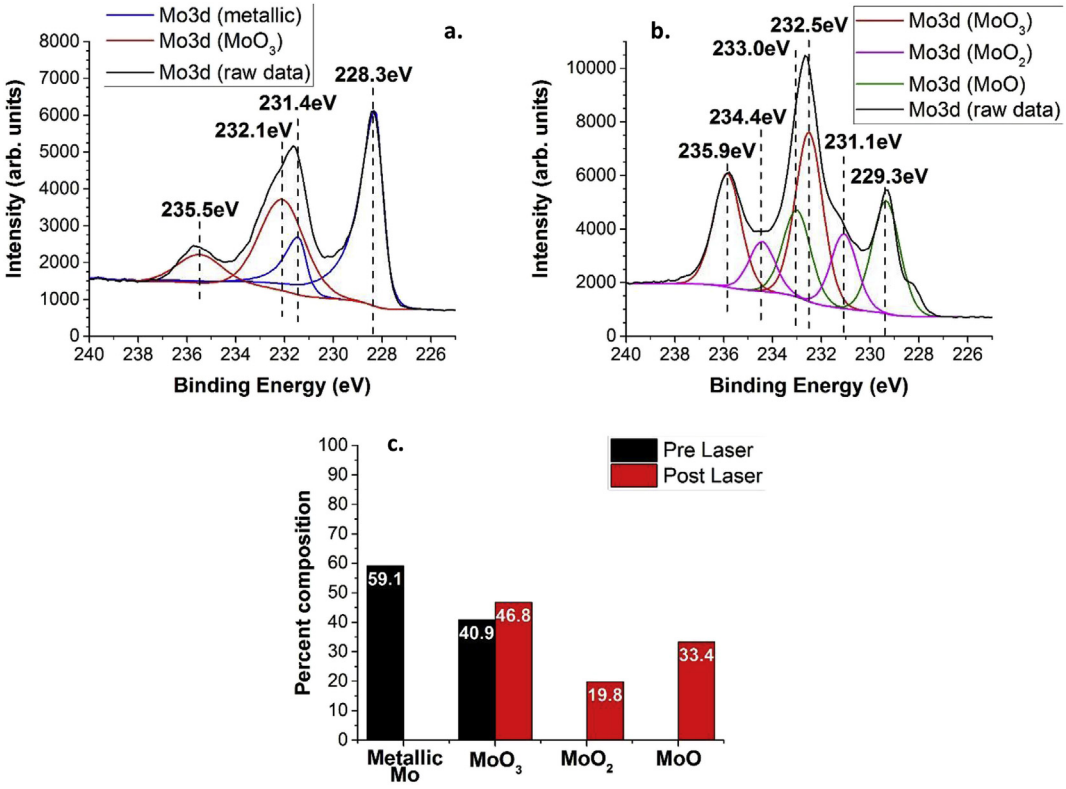

Fig. 13. XPS spectrum of Mo3d peaks for molybdenum before laser irradiation (a) and after (b). Diagram of the surface composition in percentage of molybdenum before and after laser irradiation (c). Inherent error from composition calculation is assessed around ±5%.

trioxide (MoO_3) peaks. According to Fig. 13 (c), the laser treated surface is exclusively composed of molybdenum oxides which demonstrates the formation of a laser induced oxide layer at least as deep as the analyzed depth.

Finally, XPS analysis performed before and after laser processing show the systematic presence of a native oxide layer on untextured samples and an oxide reconstructing phenomenon on laser textured samples. Local temperatures involved in the laser-matter interaction process at high repetition rate and under atmospheric conditions explain the results obtained above. Both untreated and treated samples present surface oxidation but show significant difference in contact angles. Therefore, laser induced topography under the form of self-organized periodic nanostructures appear as the main contribution to the lithium-phobicity feature of textured surfaces. Nevertheless, the laser induced oxide reconstructing may help in a lesser extent to reduce the wetting of liquid lithium on nanostructured materials. Both effects confirm results obtained in this study; namely, the higher metallo-phobicity after laser texturing of molybdenum, followed by tungsten and 304 L stainless steel.

5. Conclusion

Wetting properties of liquid metals is a technologic challenge when it comes to liquid surface PFC. Most of the time, the wetting of liquid metal onto the surface of the PFC is sought in both CPS PFC and flowing liquid metal PFC systems. Nevertheless, due to its architecture, the flowing liquid metal divertor in LiMIT requires the wettability of the liquid lithium to be controlled locally. Liquid lithium has to fully wet the inside of trenches while it's expected to not wet the periphery of trenches. The latter case is the object of this study. A 1040 nm fs laser surface texturing process was used to induce periodical self-organized micro and nanostructures (ripples) formation on three fusion relevant materials: molybdenum, tungsten, and 304 L stainless steel, and therefore created lithium-phobic surfaces. Laser parameters (fluence and number of pulses per spot) used to obtain nanostructured surfaces differed for each material. The Materials Characterization Test Stand (MCATS) chamber developed at CPMI was used to conduct liquid lithium wetting tests on laser treated materials and investigate liquid lithium contact angles depending on substrate temperature (from 200 °C to 400 °C). Depending on the material, it was shown that from 320 °C to 360 °C untreated surfaces will start to wet while nanostructured surfaces will still exhibit a lithium-phobic behavior. It is beneficial that this selective wetting regime occurs at the optimal operational temperature for liquid lithium in fusion devices, since lithium evaporation is still very low up to approximately 400 °C. Furthermore, it was shown that topography in the form of self-organized periodical nanostructures (ripples) as well as the surface chemistry in the form of oxides enrichment – both induced by a single step laser process – strongly influence the wetting degree of liquid lithium and enhance lithium phobicity at high temperatures. Finally, the mettalo-phobicity of laser treated samples for liquid lithium, observed until 400 °C paves the way for surface structuring techniques in the conception of LiMIT divertor, to aid in flow control on metal surfaces. In the near future, surfaces of divertor and limiter structures could be also texturize by ultrafast laser for effective thermal management, and prevention of material failure. This makes liquid metal divertor concepts more technologically feasible.

Acknowledgments

This work was supported by the DOE Phase II SBIR/STTR (award number DE-SC0011851) and Starfire Industries LLC. Parts of this research were carried out in the Frederick Seitz Materials Research Laboratory Central Facilities, University of Illinois, which is partially supported by the U.S. Department of Energy under Grant Nos. DEFG02-07ER46453 and DE-FG02-07ER46471.

References

[1] R.E. Nygren, F.L. Tabarés, Liquid surfaces for fusion plasma facing components—a critical review. Part I: physics and PSI, Nucl. Mater. Energy 9 (2016) 6–21.
[2] M. Ono, Lithium as Plasma Facing Component for Magnetic Research Fusion, Office of Scientific and Technical Information, Princeton Plasma Physics Laboratory, 2012.
[3] M.J. Baldwin, R.P. Doerner, Formation of helium induced nanostructure “fuzz” on various tungsten grades, J. Nucl.Mater. (2010) 165–173.
[4] R.E. Nygren, D.F. Cowgill, M.A. Ulrickson, B.E. Nelson, P.J. Fogarty, T.D. Rognlien, et al., Design integration of liquid surface divertors, Fusion Eng. Des. 72 (2004) 223–244.
[5] V. Surla, M.A. Jaworski, T.K. Gray, K. Ibano, W. Xu, M.J. Neumann, D.N. Ruzic, Lithium research as a plasma facing component material at the University of Illinois, Thin Solid Films 518 (2010) 6663–6666.
[6] I.E. Lyublinski, A.V. Vertkov, V.A. Evtikhin, Application of lithium in systems of fusion reactors. 1. Physical and chemical properties of lithium, Plasma Dev. Oper. 17 (2009) 42–72.
[7] F. Tabarés, D.T. Oyarzabal, A.B.M. Rojo, D. Alegre, T.-I. team, TJ-II experiments for testing lithium as a possible PFC for a Fusion Reactor, in: 3rd Int. Symp. Lithium Appl. Fusion Devices, 2013.
[8] A.V. Vertkov, I.E. Lyublinski, F. Tabares, E. Ascasibar, Status and prospect of the development of liquid lithium limiters for stellarotor TJ-II, Fusion Eng. Des. 87 (2012) 1755–1759.
[9] G.Z. Zuo, J. Ren, J.S. Hu, Z. Sun, Q.X. Yang, J.G. Li, et al., Liquid lithium surface control and its effect on plasma performance in the HT-7 tokamak, Fusion Eng. Des. 89 (2014) 2845–2852.
[10] R. Kaita, L. Berzak, D. Boyle, T. Gray, E. Granstedt, G. Hammett, et al., Experiments with liquid metal walls: status of the lithium tokamak experiment, Fusion Eng. Des. 85 (2010) 874–881.
[11] D.N. Ruzic, W. Xu, D. Andruczyk, M.A. Jaworski, Lithium–metal infused trenches (LiMIT) for heat removal in fusion devices”, Nucl. Fusion 51 (2011), 102002 (4pp).
[12] J.C. Schmitt, et al., Results and future plans of the Lithium Tokamak eXperiment (LTX), JNM (J. Nucl. Med.) 438 (2013) S1096–S1099.
[13] H.Y. Guo, et al., Approaches towards long-pulse divertor operations on EAST by active control of plasma–wall interactions, Nucl. Fusion 54 (1) (2014) 013002.
[14] M.A. Jaworski, N.B. Morley, D.N. Ruzic, Thermocapillary and thermoelectric effects in liquid lithium plasma facing components, J. Nucl. Mater. 390–91 (2009) 1055–1058.
[15] H.W. Kugel, et al., NSTX plasma operation with a liquid lithium divertor, Fusion Eng. Des. 87 (2012) 1724–1731.
[16] S. Mirnov, et al., Plasma-wall interactions and plasma behaviour in fusion devices with liquid lithium plasma facing components, J. Nucl. Mater. 876 (2009) 390–391.
[17] A.V. Vertkov, et al., Development of lithium CPS based limiters for realization of a concept of closed lithium circulation loop in tokamak, Fusion Eng. Des. 89 (2014) 996–2002.
[18] T.F. Lin, T.A. Palmer, K.C. Meinert, N.R. Murray, R. Majeski, Capillary wicking of liquid lithium on laser textured surfaces for plasma facing components, JNM (J. Nucl. Med.) 433 (2013) 55–65.
[19] P. Fiflis, M. Christenson, M. Szott, K. Kalathiparambil, D.N. Ruzic, Free surface stability of liquid metal plasma facing components, Nucl. Fusion 56 (2016), 106020 (10pp).
[20] M. Ono, R. Majeski, M. Jaworski, Y. Hirooka, R. Kaita, T. Gray, R. Maingi, C. Skinner, M. Christenson, D. Ruzic, Liquid lithium loop system to solve challenging technology issues for fusion power plant Nucl, Fusion 57 (2017) 116056.
[21] J. Ren, G.Z. Zuo, J.S. Hu, Z. Sun, J.G. Li, L.E. Zakharov, D.N. Ruzic, W.Y. Xu, Investigations on interactions between the flowing liquid lithium limiter and plasmas, Fusion Eng. Des. 102 (36) (2016).
[22] P. Fiflis, T.W. Morgan, S. Brons, G.G. Van Eden, M.A. Van Den Berg, W. Xu, D. Curreli, D.N. Ruzic, Performance of the lithium metal infused trenches in the magnum PSI linear plasma simulator, Nucl. Fusion 55 (11) (2015) 113004.
[23] W. Xu, P. Fiflis, M. Szott, K. Kalathiparambil, S. Jung, M. Christenson, I. Haehnlein, A. Kapat, D. Andruczyk, D. Curreli, D.N. Ruzic, Vertical flow in the thermoelectric liquid metal plasma facing structures (TELS) facility at Illinois, JNM (J. Nucl. Med.) 463 (2015) 1181–1185.
[24] P. Fiflis, A. Press, W. Xu, D. Andruczyk, D. Curreli, D.N. Ruzic, Wetting properties of liquid lithium on select fusion relevant surfaces, Fusion Eng. Des. 89 12 (2014) 2827–2832.
[25] R. Buividas, M. Mikutis, S. Juodkazis, Surface and bulk structuring of materials by ripples with long and short laser pulses: recent advances, PQE 38 (2014) 119–156.
[26] J. Bonse, J. Krüger, S. Höhm, A. Rosenfeld, Femtosecond laser-induced periodic surface structures, J. Laser Appl. 24 4 (2012).

[27] P. Bizi Bandoki, S. Valette, E. Audouard, S. Benayoun, Time dependency of the hydrophilicity and hydrophobicity of metallic alloys submitted to femtosecond laser irradiations, Appl. Surf. Sci. 273 (2013) 399–407.
[28] S. Hammouti, A. Pascale-Hamri, N. Faure, B. Beaugiraud, M. Guibert, C. Mauclair, S. Benayoun, S. Valette, Wear rate control of peek surfaces modified by femtosecond laser, Appl. Surf. Sci. 357 (2015) 1541–1551.
[29] V. Dumas, A. Guignandon, L. Vico, C. Mauclair, X. Zapat, M.T. Linossier, W. Bouleftour, J. Granier, S. Peyroche, J.C. Dumas, H. Zahouani, A. Rattner, Femtosecond laser nano/micro patterning of titanium influences mesenchymal stem cell adhesion and commitment, Biomed. Mater. 10 5 (2015).
[30] Xxx Sedao, R. Torres, T. Sarnet, P. Delaporte, M. Sentis, Laser textured black silicon solar cells with improved efficiencies, Adv. Mater. Res. 321 (2011) 240–245.
[31] J. Krüger, W. Kautek, Ultrashort pulse laser interaction with dielectrics and polymers, Adv. Polym. Sci. 168 (2004) 247–290.
[32] J.M. Liu, Simple technique for measurements of pulsed Gaussian-beam spot sizes, Opt. Lett. 7 5 (1982) 196–198.
[33] D. Nečas, P. Klapetek, Gwyddion: an open-source software for SPM data analysis, Cent. Eur. J. Phys. 10 (1) (2012) 181–188.
[34] T. Furukawa, Y. Hirakawa, H. Kondo, T. Kanemura, E. Wakai, Chemical reaction of lithium with room temperature atmosphere of various humidities, Fusion Eng. Des. 98 (2015) 2138–2141.
[35] S.A. Krat, A.S. Popkov, Yu M. Gasparyan, A.A. Pisarev, P. Fiflis, M. Szott, M. Christenson, K. Kalathiparambil, D.N. Ruzic, Wetting properties of liquid lithium on lithium compounds, Fusion Eng. Des. 117 (2017) 199–203.
[36] M. Szott, Flow Control and Associated Technologies to Advance the Application of TEMHD-driven Liquid Lithium in Fusion Devices, Master's thesis, University of Illinois at Urban Champaign, 2016.
[37] A.F. Stalder, G. Kulik, D. Sage, L. Barbieri, P. Hoffmann, A snake-based approach to accurate determination of both contact points and contact angles, Colloids Surf., A 2861–3 (2006) 92–103.
[38] A.P. Grosvenor, B.A. Kobe, M.C. Biesinger, N.S. McIntyre, Investigation of multiplet splitting of Fe 2p XPS spectra and bonding in iron compounds, Surf. Interface Anal. 36 (2004) 1564–1574.
[39] M.C. Biesinger, C. Brown, J.R. Mycroft, R.D. Davidson, N.S. McIntyre, X-ray photoelectron spectroscopy studies of chromium compounds, Surf. Interface Anal. 36 (2004) 1550–1563.
[40] Perry A. Spevack, N.S. McIntyre, A Raman and XPS investigation of supported molybdenum oxide thin films. 1. Calcination and reduction studies, J. Phys. Chem. 97 (1993), 11020–11021 1030.
[41] C. Bittencourt, A. Felten, F. Mirabella, P. Ivanov, E. Llobet, M.A.P. Silva, L.A.O. Nunes, J.J. Pireaux, High-resolution photoelectron spectroscopy studies on WO3 films modified by Ag addition, J. Phys. Condens. Matter 17 (43) (2005).
[42] J. Bonse, A. Rosenfeld, J. Krüger, On the role of surface plasmon polaritons in the formation of laser-induced periodic surface structures upon irradiation of silicon by femtosecond laser pulses, J. Appl. Phys. 106 (2009) 104910.
[43] G.A. Martsinovskii, G.D. Shandybina, D.S. Smirnov, S.V. Zabotnov, L.A. Golovan, V. Yu Timoshenko, P.K. Kashkarov, Ultrashort excitations of surface polaritons and waveguide modes in semiconductors, Opt.Spectrosc. 105 (2008) 67–72.
[44] J. Reif, F. Costache, M. Henyk, S.V. Pandelov, Ripples revisited: non-classical morphology at the bottom of femtosecond laser ablation craters in transparent dielectrics, Appl. Surf. Sci. 197–198 (2002) 891–895.
[45] A. Borowiec, H.K. Haugen, Subwavelength ripple formation on the surfaces of compound semiconductors irradiated with femtosecond laser pulses, Appl. Phys. Lett. 82 (2003) 4462–4464.
[46] D. Dufft, A. Rosenfeld, S.K. Das, R. Grunwald, J. Bonse, Femtosecond laser-induced periodic surface structures revisited: a comparative study on ZnO, J. Appl. Phys. 105 (2009), 034908-1–;034908–034909.
[47] E.S. Gadelmawla, M.M. Koura, T.M.A. Maksoud, I.M. Elewa, H.H. Soliman, Roughness parameters, J. Mater. Process. Technol. 123 (1) (2002) 133–145.
[48] D.H. Kam, S. Bhattacharya, J. Mazumder, Control of the wetting properties of an AISI 316L stainless steel surface by femtosecond laser-induced surface modification, J. Micromech. Microeng. 22 (2012), 105019 (6pp).
[49] J. Long, P. Fan, D. Gong, D. Jiang, H. Zhang, L.Li, M. Zhong, Superhydrophobic surfaces fabricated by femtosecond laser with tunable water adhesion: from Lotus leaf to rose petal, ACS Appl. Mater. Interfaces 7 (2015) 9858–9865.
[50] T. Young, An essay on the cohesion of fluids, Trans. R. Soc. Lond. 95 (1805) 65.
[51] R.N. Wenzel, Resistance of solid surfaces to wetting by water, Ind. Eng. Chem. 28 (1936) 988–994.
[52] C.S. Baxter, Wettability of porous surfaces, Trans. Faraday Soc. 40 (1944) 546–551.
[53] R.K. Kramer, J.W. Boley, H.A. Stone, J.C. Weaver, R.J. Wood, Effect of microtextured surface topography on the wetting behavior of eutectic Gallium–Indium alloys, Langmuir 30 (2014) 533–539.
[54] F. Delannay, L. Froyen, A. Deruyttere, The wetting of solids by molten metals and its relation to the preparation of metal-matrix composites, J. Mater. Sci. 22 (1987) 1–16.
[55] V.P. Veiko, M.V. Yarchuk, I. Ivanov, Study of low-threshold mechanisms for modifying the structure of thin chromium films under the action of supershort laser pulses, J. Opt. Technol. 78 8 (2011) 512–518.